Surface trace doping of Na enhancing structure stability and adsorption properties of $Li_{1.6}Mn_{1.6}O_4$ for Li^+ recovery

Fangren Qian;[1, 2, 3] Bing Zhao;[1, 2, 3] Min Guo;[1, 2] Zhijian Wu[1, 2]; Wuzong Zhou[4]; Zhong Liu;*[1, 2]

[1] Key Laboratory of Comprehensive and Highly Efficient Utilization of Salt Lake Resources, Qinghai Institute of Salt Lakes, Chinese Academy of Sciences, Xining 810008, China

[2] Key Laboratory of Salt Lake Resources Chemistry of Qinghai Province, Xining 810008, China

[3] University of Chinese Academy of Sciences, Beijing 100049, China

[4] School of Chemistry, University of St Andrews, St. Andrews, Fife KY16 9ST United Kingdom

**Corresponding author, E-mail address: liuzhong@isl.ac.cn*

Abstract: $Li_{1.6}Mn_{1.6}O_4$ (LMO) is a dominant adsorbent for lithium recovery from solutions resulted from its high theoretical adsorption uptake and a low loss rate of Mn, which can potentially be further improved by trace doping. We achieve stable cycling and high adsorption capacity of $Li_{1.6}Mn_{1.6}O_4$ from aqueous lithium resources by Na doped (LMO-Na). The Mn dissolution is decreased from 5.4% (bare adsorbent) to 4.4%, and the uptake is increased from 33.5 mg/g to 33.9 mg/g (C_{Li+}: 24 mmol/L). Furthermore, DFT calculations predict that Na replace for Li at 16d sites, result in an enhancement of the Li^+ adsorption rate and structure stability of LMO. The loss rate of Mn in cycling process is restrained by Na doped, which may result from reducing the content of low valent Mn^{3+} and improving the structural stability of material. The effect of Na substitution on adsorption capacity and structure stability is discussed.

Keywords: $Li_{1.6}Mn_{1.6}O_4$; adsorption; Mn dissolution, DFT calculations

1. Introduction

Recently, the constantly increasing lithium consumption for Li-ion batteries has led to a pressing demand for new technologies of lithium recovery [1-3], from solid ores and aqueous lithium resources. Especially, the brines have a large storage of Li [4, 5]. However, there are many interfering ions and the concentration of Li^+ is extreme low in these aqueous resources. Therefore, it is appropriate to extract lithium from salt lakes by an adsorption method with a high ion selectivity [6].

Compounds derived from manganese oxides with a spinel crystal structure, such as $LiMn_2O_4$ [7, 8], $Li_4Mn_5O_{12}$ [9, 10], $Li_{1.6}Mn_{1.6}O_4$ [4, 11, 12], have been paid increasing attention result from high adsorption uptake of Li^+ and excellent ion selectivity. But these adsorbents suffer from considerable dissolution of Mn during the desorption process [13]. Many methods, such as surface-modification [14] and doping [15], have been used to enhance the cycle stability of a typical manganese oxide based adsorbent. Doping has been regarded as the most widespread and valid method to enhance cycle property of $Li_{1.6}Mn_{1.6}O_4$ (LMO) among the different ways. The $(Li_{0.5}Zn_{0.5})[Li_{0.5}Mn_{1.5}]O_4$ was obtained by Feng et al. via a co-precipitation route, and the desorption rate of Li^+ was reduced after HCl treatment [16]. Chitrakar et al. [17] synthesized $Li_4Fe_xMn_{5-x}O_{12}$ and indicated that the dissolution of Mn reduced when the Fe/Mn ratio increased, and uptake of Li^+ is increased. However, foreign elements enter into LMO for Li^+ adsorption were rarely studied [13].

In the present work, Na-doped $Li_{1.6}Mn_{1.6}O_4$ with various doped amounts were

prepared and the structures were tested by different methods. The improved Li^+ adsorption and Mn stability of the LMO-Na adsorbents were examined.

2. Experimental

2.1 Synthesis of materials

$(Li_{1-x}Na_x)_{1.6}Mn_{1.6}O_4$ (x = 2%, 5%, 10%, 15%), denoted LMO-Na-R (R is the Na content represent to x), were prepared by calcinating mixtures of NaCl and $LiMnO_2$ at 350ºC (24 h) and the $LiMnO_2$ was obtained by hydrothermal way. The prepared process was according to previous work of our lab [18]. $(H_{1-x}Na_x)_{1.6}Mn_{1.6}O_4$ (HMO-Na-R) were obtained after Li^+ desorption in HCl solution (24 h). The r-LMO-Na-R refer to the materials of Li^+ re-intercalated.

2.2 Characterization of specimens

The XRD and SEM are used to investigate the structure and morphologied of materials. The STEM used to obtained more information of structure. BET surface area and pore diameter distributions were studied by N_2 ad/desorption. The amounts of Mn^{2+} and Li^+ were tested using ICP conducted on inductively coupled plasma (Optima 7000DV). DSC-TG of the materials was used to investigte the weight change during the heating process. X-ray photoelectron spectroscopy were used to study the valence state of Mn and FT-IR were carried out on a Bruker Tensor 27 spectrometer.

2.3 Li^+ uptake performance

Li^+ uptake experiments were carried out by adding 0.1 g HMO-Na-2% to 100 mL LiCl solution for 48 h at different amounts (6, 12, 24 mmol/L) and temperature (25, 35, 45ºC). The pH of the LiCl solutions were adjust using HCl/KOH. The Li^+ amounts was

tested using ICP. Li^+ uptake capacity of HMO-Na-2% was confirmed according to Eq. (1) [19]:

$$q_e = \frac{V}{m}(C_0 - C_e) \quad (1)$$

The q_e (mg/g) signify the Li^+ adsorption uptake; m (g) denotes the mass of the HMO-Na-R; C_0 and C_e refer Li^+ amounts of the before and after adsorption (mg/L); V (L) represent the solution volume.

In order to study the selectivity for Li^+, 0.1 g HMO-Na-2% was added to a single MCl and mixed solution containing M ions (M = Li^+, Na^+, K^+, Rb^+, Cs^+) for 48 h at pH 12. To evaluate the adsorption behaviors of the obtained materials and explore its practicability, the relevant practicable experiments were performed on adding 0.1 g HMO-Na-2% to the Lagoco brine (100 mL). The concentrations of various ions were confirmed by ICP. The relevant parameters were confirmed by Eq. (2) and (3) respectively [20].

$$K_d = (C_0 - C_e)\ \frac{V}{mC_e} \quad (2)$$

$$\alpha_M^{\mathrm{Li}} = \frac{K_{Li}}{K_d} \quad (3)$$

$$C_F = q_{e_M}/C_{0_M} \quad (4)$$

Where the K_d and K_{Li} denote the distribution coefficient of other ions and Li^+; C_F is the concentration factor, α_M^{Li} refer separation factor.

2.4 The loss rate of Mn

The experiments of Mn dissolution were carried out by adding o.1g LMO-Na-R into HCl solution (C_{HCl}: 0.6 mol/L, *V:* 100 mL) containing some H_2O_2 and stirring 100 mL HCl solution (0.3, 0.6 and 1.2 mol/L) containing 0.1 g LMO-Na-2% for 24 h at

different temperature (25, 35, 45°C). The amounts of Li^+ and Mn^{2+} were detected by ICP. The ratio of desorption Li and Mn were confirmed according to Eq. (5) [21]:

$$r = C_i/S \quad (5)$$

The *r* denotes loss ratio of Li or Mn; C_i and S signify amounts of Li^+ or Mn^{2+} in solution and solid sample.

2.5 DFT calculations

First-principles calculations according to DFT were performed on VASP and were used to investigate the physicochemical performances of materials [22]. The way was based on the previous similar work [23] and placed in Supporting Information.

3 Results and discussion

3.1 characterization of obtained manganese oxides

Fig. 1 displays the XRD patterns of as-obtained manganese oxide derived products. The synthesized $LiMnO_2$ has a high purity and crystallinity (Fig. 1a) [24]. LMO-Na-2% is single phase, which belong to spinel strycture. NaCl appears in the LMO with higher Na doped (5%, 10% and 15%), implying the excess Na will not enter into LMO crystal lattice (Fig. 1b). All the LMO-Na-2%, HMO-Na-2% and r-LMO-Na-2% indicate spinel structure (Fig. 1c), implying the obtained manganese oxides poesses high structure stability. The interplanar spacing (*d*) of LMO-Na-2% in (111) plane is 4.72 Å, and decreased to 4.67 Å in HMO-Na-2%, in turn increased to 4.70 Å in r-LMO-Na-2%, which is result from the H^+/Li^+ ion exchange [25].

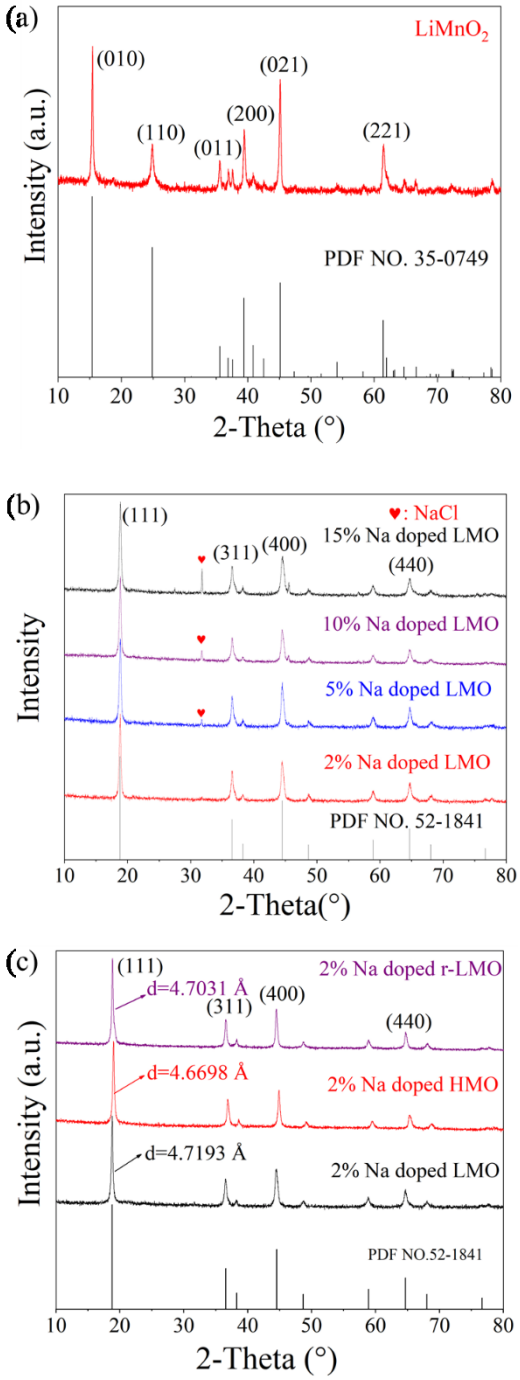

Fig. 1. XRD patterns of obtained materials. (a): $LiMnO_2$; (b): LMO-Na-R; (c): LMO-Na-2%, HMO-Na-2%, and r-LMO-Na-2%.

Similar morphologies of LMO-Na-2%, HMO-Na-2% and r-LMO-Na-2% as depicted in Fig. 2(a-d). The results indicate the morphologies of obtained manganese oxide have little change during the ad/desorption process. Further elemental mappings of the local region over a r-LMO-Na-2% particle indicate an overall homogeneous

distribution of the elements O, Mn and Na (Fig. 2e). The STEM with atomic resolution was used to obtained more structure information of the Na-doped LMO, the annular bright field (ABF) and high-angle annular dark-field (HAADF) images of LMO-Na-2% as depicted in Fig. 2(f-g). The results indicate no lattice distortion caused by Na doping and the Na atom appear in surface, indicating Na doped occurs in the surface area without a deep penetration into the particles bulk [26]. By The particle size distribution and HAADF image of powders with different granulometry (Fig. S1, supporting information), we also can confirm that the Na atoms may substitute Li on surface.

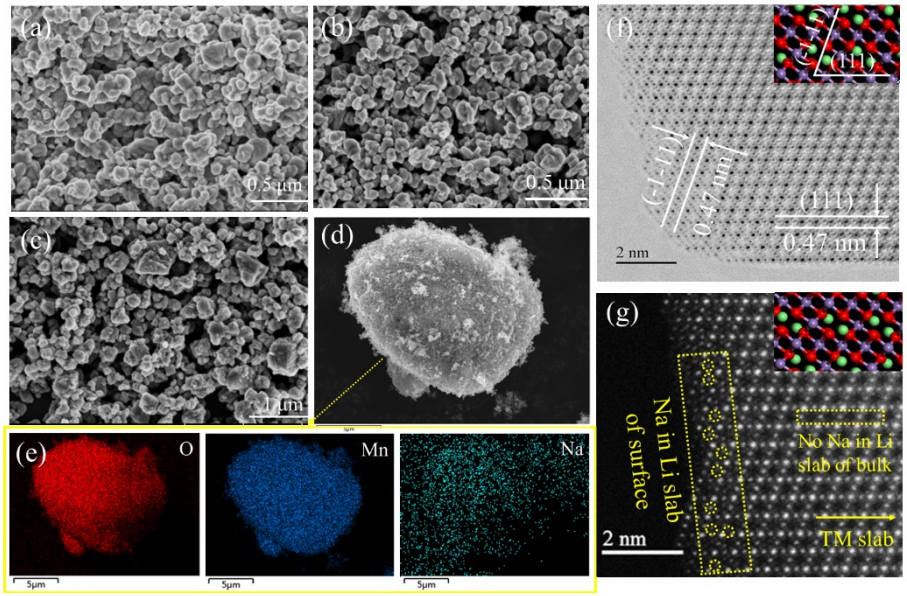

Fig. 2. SEM of (a) LMO-Na-2%; (b) HMO-Na-2% (c-d) r-LMO-Na-2%; (e) elemental mapping from (d); (f) ABF and (g) HAADF images of LMO- Na-2%.

Fig. 3. shows FT-IR spectra of the as-prepared LMO-Na-2% and HMO-Na-2%. In LMO-Na-2%, the bands at 3441.5 and 1632 cm^{-1} are due to O-H vibrations [27, 28]. The band at 1072.9 cm^{-1} is Li-O from asymmetric stretching vibration [29]. The peaks at 648.6 and 515.1 cm^{-1} belong to Mn(IV)-O and Mn(III)-O [30, 31]. All the bands are appeared in HMO-Na-2% with a slight transfer. The band at 1071.3 cm^{-1} is also exist in HMO-Na-2%, indicating a small amount of Li in the HMO. Furthermore, a new band observed in HMO at 908.3 cm^{-1}, which may due to the lattice vibration of protons,

implying ion-exchange between H^+ and Li^+ exist in the HCl treatment process [27]. The desorption process has little effect on the peaks of Mn-O, showing that the high stability of [MnO_6] octahedron during the desorption process consistent with XRD results (Fig. 1c).

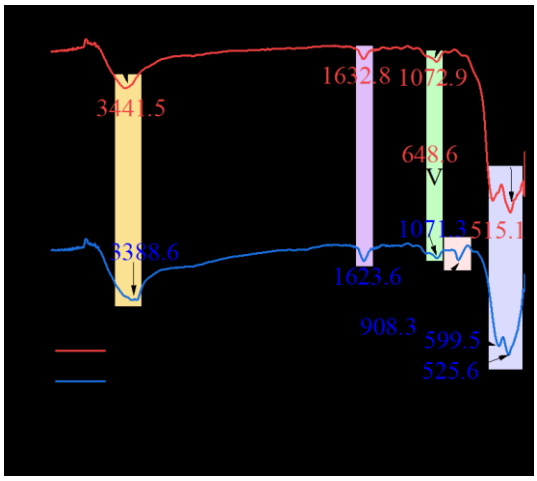

Fig. 3. FT-IR patterns of 2% Na-doped manganese oxides.

The fitting results of Mn $2p_{3/2}$ of LMO-Na-2%, HMO-Na-2%, r-LMO-Na-2% and 2-HMO-Na-2% are depicted Fig. 4(a-b). The bands of 642.7 eV and 642.1 eV are result from [$Mn^{4+}O_6$] and [$Mn^{3+}O_6$], respectively [32]. In addition, the amounts of Mn^{3+} is 14% in LMO-Na, and it is decreased to 10% in HMO-Na after HCl treatment. The amount of Mn^{3+} is maintain 10% in r-LMO-Na after Li^+ adsorption process, and it is further reduced to 8% after second HCl treatment (2-HMO-Na), showing a possible loss of Mn^{3+} during the desorption process. The amounts of Mn^{4+} in LMO is increased by trace Na doped (Fig. S3, supporting information), which may due to the Na replace Li sites and improving the average valence state of Mn in LMO. The curves of O 1s as depicted in Fig. 4(c-d) and the peak of -OH about 531 eV in HMO is obviously stronger than LMO, result from ion-exchange between H^+ and Li^+ [25]. The bands at near 529.8 eV

are similar between LMO and HMO, imply the structure of [MnO_6] is stable, which is in line with the FT-IR spectra from Fig. 3 [33].

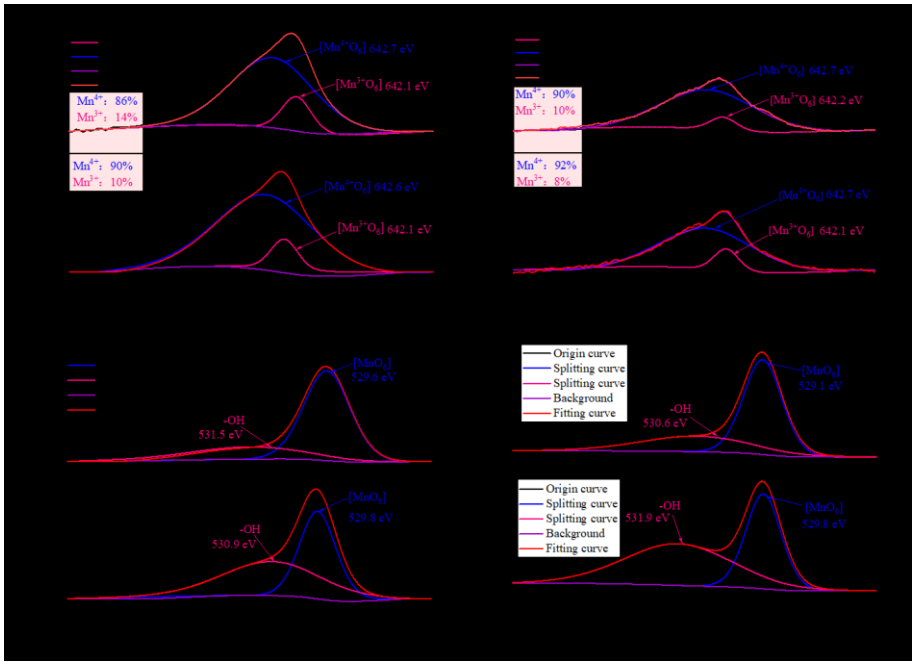

Fig. 4. XPS patterns of 2% Na-doped LMO, HMO, r-LMO and 2-HMO with the fitting results of (a-b) Mn $2p_{3/2}$ and (c-d) O 1s (2-HMO is the adsorbent in second cycle).

3.2 Adsorption properties

3.2.1 Effect of different doping level on Li^+ uptake

The amounts of doping is an vital factor which effects on Li^+ adsorption capacity, and the results are depicted in Fig. 5(a). Compare to bare HMO (25.9 mg/g), the Li^+ uptake is improved by Na doped (27.3 mg/g), and reduces with the doping level enhances, implying the Na doping cannot exceed 5% in line with the results of XRD. The excessive Na will change the lattice constant, resulting in the ion-exchange between Li^+ and H^+ became more difficulties. The Li^+ uptake enhanced by 2% Na doping may result from inhibiting the decay of capacity in cycle process [34]. Beside this, the adsorption rate of HMO-Na-2% (blue line) is faster than others in 12 h may not due to the specific surface area (Fig. S4). Therefore, we will pay more attention on

2% Na doped in the following work.

Fig. 5(b) presents the Li^+ uptake behavior of HMO and HMO-Na-2% at different Li^+ concentrations. It can be observed that the Li^+ uptake of HMO-Na-2% is up to 27.2 mg/g while the HMO is 25.8 mg/g at initial Li^+ concentration of 6 mmol/L. The Li^+ adsorption capacity of HMO-Na-2% and HMO increase to 33.9 and 33.5 mg/g at a solution of Li^+ concentration of 24 mmol/L. The results show that the Li^+ uptake capacity of HMO-Na-2% is higher than HMO at different concentrations of Li^+.

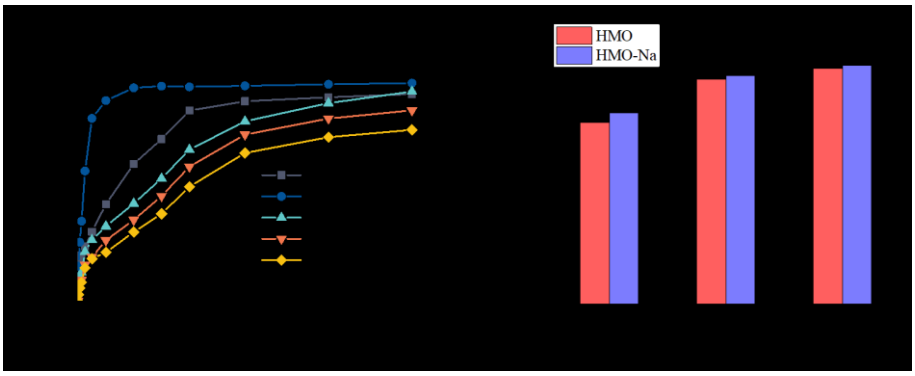

Fig. 5. The adsorption capacity of (a) HMO with different Na^+ doping amounts and (b) bare and Na doped HMO at different initial Li^+ concentration (Adsorbent dosage: 1 g/L, pH 12, *T*: 25°C).

3.2.2 Li^+ intercalation/de-intercalation mechanisms

The Li^+ insertion sites of $Li_{1.6}Mn_{1.6}O_4$ can be divide into two parts: redox-type sites and ion-exchange sites [35]. The percentage of each part are concerned with the synthesis process. The valence state of Mn in the prepared materials have a vital effect on the formation of the insertion sites, which the proportion of ion-exchange sites increased with the amounts of Mn(IV) increasing. The schematic representation in Fig. 6 indicates the Li^+ extraction/insertion by the composite mechanism in LMO, which can explain in detail the Li^+ ad/desorption behaviors in solution [36].

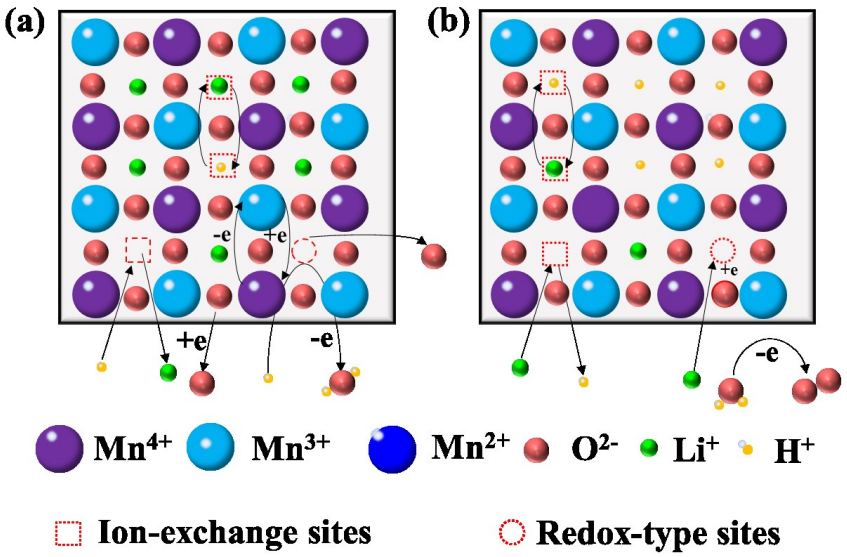

Fig. 6. Schematic representation in LMO by the composite mechanism (a) Li^+ extraction reactions and (b) Li^+ insertion reactions.

3.2.2 Effect of pH on Li^+ adsorption

The pH has important influence on Li^+ uptake of HMO-Na-2% and the results are depicted in Fig. 7. Li^+ uptake is 0.85 mg/g at pH = 3, and reach to 4.9 mg/g (pH: 7). The Li^+ uptake improves to 15 and 27 mg/g at pH 11 and 12, which may result from the pH increases will accelerate the ion-exchange between Li^+ and H^+ by Eq. (6) [37].

$$H_{1.6}Mn_{1.6}O_4 + Li^+ \rightleftharpoons Li_{1.6}Mn_{1.6}O_4 + H^+ \quad (6)$$

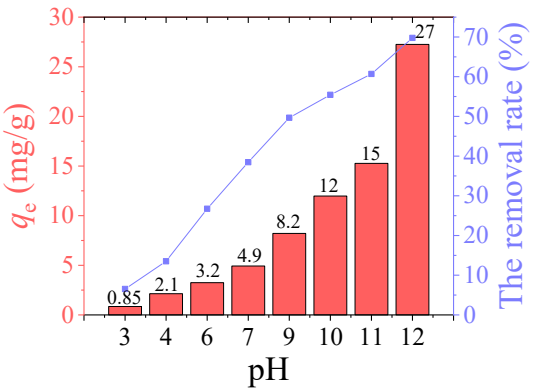

Fig. 7. Influence of pH on Li^+ uptake.

3.2.3 Adsorption isotherms

To illustrate the Li^+ adsorption behaviors, the Langmuir, Freundlich, Dubinin-Radushkevich (D-R) and Temkin isotherm models were used to fit the adsorption behavior [38-40]:

$$\frac{C_e}{q_e} = \frac{1}{q_m b} + \frac{C_e}{q_m} \tag{7}$$

$$\ln q_e = \ln k_F + \frac{1}{\mathrm{n}} \ln C_e \tag{8}$$

$$\ln q_\mathrm{e} = \ln q_\mathrm{m} - \beta_\mathrm{DR} \varepsilon^2 \tag{9}$$

$$q_\mathrm{e} = \frac{RT}{b} \ln K_T + \frac{RT}{\mathrm{b}} \ln \mathrm{C_e} \tag{10}$$

Where C_e indicates the final concentration of Li^+ (mg/L), q_e and q_m signifies the equilibrium and theoretical maximal uptake (mg/g), b shows the Langmuir constant (L/mg), k_F (mg/g) and n represent the Freundlich constants. β_DR ($\mathrm{mol^2 J^{-2}}$) denote the D-R constant, ε imply the Polanyi potential ($\varepsilon = RT\ln(1 + 1/C_\mathrm{e})$), R indicate the molar gas coefficient (8.314 J $\mathrm{mol^{-1}\ K^{-1}}$), T signify absolute temperature (K), b denote the Temkin constant which is connected with uptake heat (J/mol), and K_T show the Temkin isotherm coefficient. According to β_DR, the average uptake energies E (kJ/mol) was confirmed by Eq. (11) [40]:

$$E = \frac{1}{\sqrt{2\beta_{DR}}} \tag{11}$$

The fitted results as shown in Fig. 8(a-b), indicating Li^+ adsorption process fits well by the Langmuir result from higher R^2 (0.99) than Freundlich model (0.96), implying Li^+ adsorbed on adsorbent is a monolayer uptake [19]. The relevant parameters in detail as shown in Table 1.

Despite the Langmuir model indicates the formation of a chemical bond, and the

obtained parameters do not offer any information about interaction between adsorbent and adsorbate. In order to illustrate the property of uptake process, the uptake behaviors were fitted by the Dubinin-Radushkevich and Temkin isotherm models (Eq. (9) and (10)). The fitted results as depicted in Fig. 8 and the calculated parameters are listed in Table 2. The values of the b and E calculated by Dubinin-Radushkevich are lower than 80 and 8 kJ/mol (Table 2), which benefit to the ad/desorption process by ion-exchange [40, 41].

The Li^+ uptake process of HMO-Na-2% at different temperature (25°C, 35°C, 45°C) as shown in Fig. S5. The Li^+ uptake is improved with temperature increased, implying the uptake is endothermic [37].

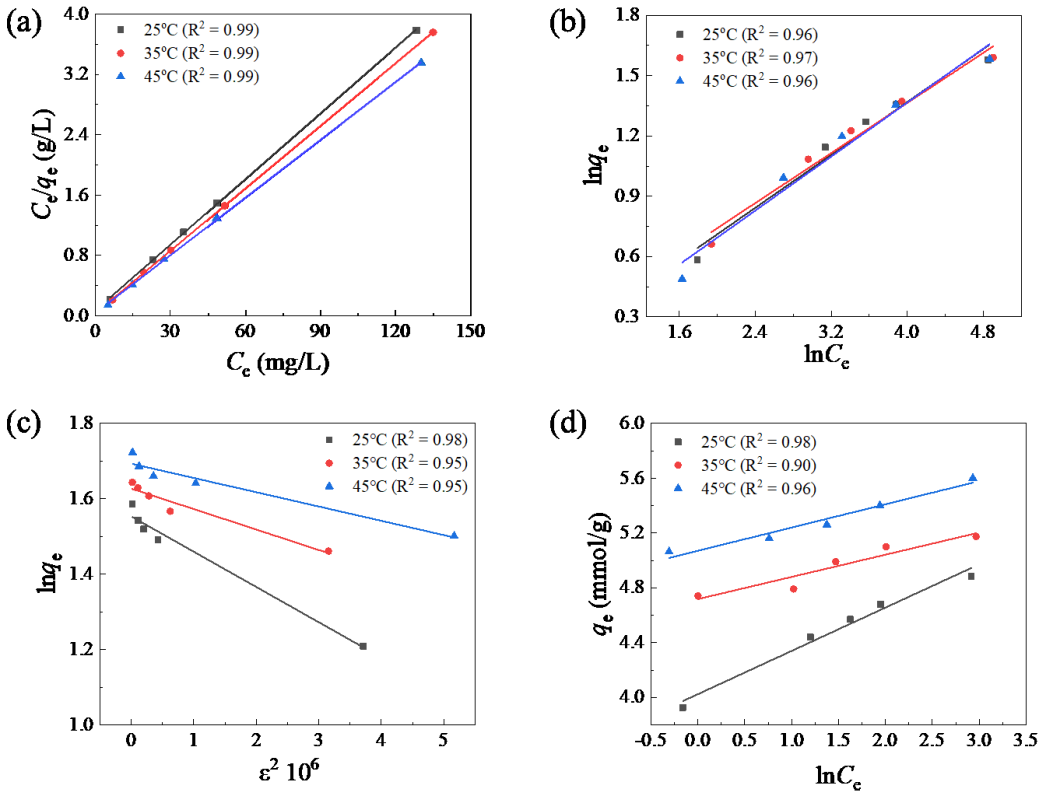

Fig. 8. (a) Langmuir, (b) Freundlich isotherm, (c) Dubinin-Radushkevich and (d) Temkin isotherm models of Li^+ adsorption process.

Table. 1. Relevant parameters base on Langmuir and Freundlich models (T = 25℃).

Material	Langmuir			Freundlich		
	q_m (mg/g)	b (L/mg)	R^2	k_F (mg/g)(L/mg)$^{1/n}$	n	R^2
HMO-Na-2%	32.7	1.13	0.99	25.7	18.6	0.96

Table. 2. The parameters fitted by Dubinin-Radushkevich and Temkin models.

	Dubinin-Radushkevich				Temkin		
Material	T (K)	q_m (mg/g)	E (kJ/mol)	R^2	k_T (L/g)	b (kJ/mol)	R^2
HMO-Na-2%	298.15	32.8	2.31	0.98	2.54	7.85	0.98
	308.15	35.3	3.03	0.95	3.37	15.83	0.90
	318.15	37.7	3.63	0.95	3.40	15.60	0.96

3.2.4 Adsorption kinetics

The Li^+ uptake behaviors on HMO-Na-2% ware fitted base on the pseudo-first-order, pseudo-second-order and intra particle diffusion models [42, 43]:

$$\ln(q_e - q_t) = \ln q_e - k_1 t \tag{12}$$

$$\frac{t}{q_t} = \frac{1}{k_2 q_e^2} + \frac{t}{q_e} \tag{13}$$

$$q_t = k_n t^{0.5} + C_n \tag{14}$$

The q_e and q_t denotes the adsorption capacity (mg/g) at equilibrium and a time t (min); the k_1 (min^{-1}) and k_2 ($g \cdot mg^{-1} \cdot min^{-1}$) indicates pseudo first-order and pseudo-second-order uptake constants, respectively. k_n ($mol \cdot g^{-1} min^{\cdot 0.5}$) show the diffusion rate constant of each process (n = 1, 2, 3).

The fitting results and obtained parameters as depicted in Fig. 9 and Table 3. The

R^2 (0.99) of the pseudo-second-order was higher than the pseudo-first-order model (R^2 = 0.74) and the $q_{e,cal}$ confirmed by the pseudo-second-order is closer to $q_{e,exp}$, indicating the Li^+ uptake is controlled by the chemical process.

The models of intra particle diffusion at different initial Li^+ concentration and the k_1, k_2 and k_3 as depicted in Fig. 9(c). The first process had a sharp slope, implying a rate-controlling process, which it was the migrate of Li^+ from the solution to the surface of adsorbent. The second process had a lower slope and it was gradual adsorption process, indicating a rate-limiting step, which it was Li^+ from surface of adsorbent diffusion into pores. The third step was the equilibrium process, which intraparticle diffusion began to slow down and the Li^+ adsorption reach to equilibrium.

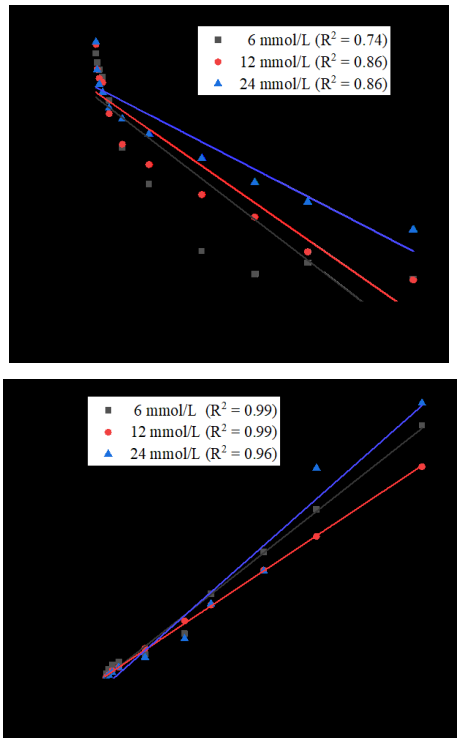

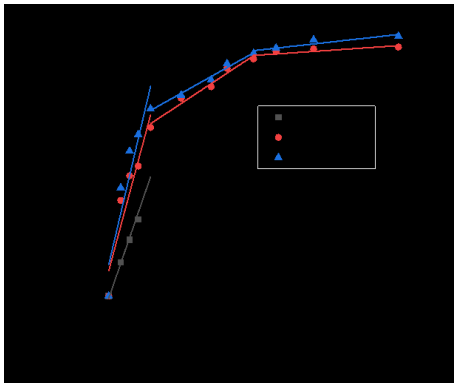

Fig. 9. (a) pseudo first-order; (b) pseudo-second-order and (c) intra particle diffusion models for Li^+ adsorption process (T = 25°C C_{Li+} = 6 mmol/L).

Table 3. Related parameters of kinetic models.

Materials	pseudo-first-order				pseudo-second-order		
	$q_{e,exp}$ (mg/g)	k_1 (min^{-1})	$q_{e,cal}$	R^2	k_2 (min^{-1})	$q_{e,cal}$ (mg/g)	R^2
HMO-Na-2%	27.3	0.00502	19.2	0.74	0.001309	27.5	0.99

3.2.5 Adsorption selectivity

The existence of interfering ion has some influence on the Li^+ uptake behaviors due to the concentration of the co-existing ions are higher than Li^+ in salt lakes. The ions (Li^+, Na^+, K^+, Rb^+, Cs^+) uptake of HMO-Na-2% in a pure and mixed solution as shown in Fig. 10. Li^+ uptake capacity by Na doped is 3.79 mmol/g in a pure LiCl solution, which is higher slightly than mixed solution (3.75 mmol/g), indicating the HMO-Na-2% possess high selectivity for Li^+. The K_d and α_M^{Li} of various ions as depicted in Table 4 and the order is $Li^+ \gg Na^+ > K^+ > Rb^+ = Cs^+$, which may result from ion radius of Li^+ (0.059 nm) is fit to the porous channel of HMO-Na-2%, and other ions with larger cannot enter into the adsorbent but adsorbed merely on surface [44].

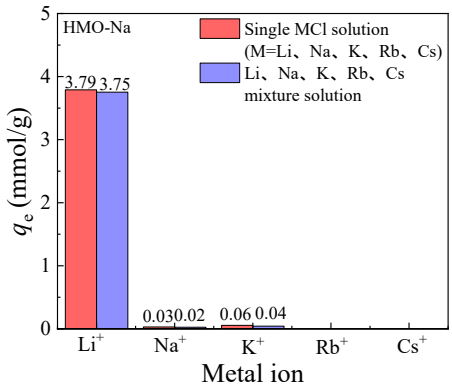

Fig. 10. Adsorption of HMO-Na-2% for various monovalent cations.

Table 4. Related parameter in selectivity experiments of HMO-Na-2%.

Cations	q_e (mmol/g)	K_d (mL/g)	α_M^{Li}
Li^+	3.3	1171.61	1
Na^+	0.022	36.2	32.4
K^+	0.066	4.78	245.1
Rb^+	0	0	-
Cs^+	0	0	-

The Li^+ uptake property of obtained materials in the Lagoco salt lake was studied, and the results as depicted in table 5. The equilibrium Li^+ uptake up to 2.71 mmol/g, which was higher obviously than Mg^{2+} (0.016 mmol/g) and Ca^{2+} (0.002 mmol/g), implying that the obtained adsorbent possesses excellent selectivity of Li^+ and Mg^{2+} in Lagoco salt lake. The order of K_d was $Li^+ > Ca^{2+} > K^+ > Mg^{2+} > Na^+$, indicating that the adsorbent by Na doped is an excellent candidate for Li^+ recovery from solution containing Li^+.

Table 5. Selectivity of HMO-Na-2% in Lagoco salt lake.

ions	C_0 (mmol/L)	C_e (mmol/L)	q_e (mmol/g)	C_F (mL/g)	K_d (mL/g)	$\alpha_{Li/M}$
Li^+	37.69	34.98	2.71	71.87	77.43	1
Na^+	699.57	699.35	0.22	0.31	0.31	249.09
K^+	62.36	62.11	0.24	3.90	3.91	19.79
Mg^{2+}	33.01	32.99	0.016	0.50	0.50	155.25

Ca^{2+}	0.539	0.537	0.002	4.63	4.65	16.66

3.2.6 Regeneration performance

Fig. 11 indicates the Li^+ uptake and loss rate of Mn in regeneration process. The fading of Li^+ adsorption and Mn loss are obvious in initial regeneration process, resulting from existence of $LiMnO_2$. In addition, the uptake of Li^+ still keep 87% after the sixth regeneration. The loss rate of Mn is below 5% in each subsequent regeneration. The results imply that the ion-sieve by Na doped have high adsorption capacity and structure stability.

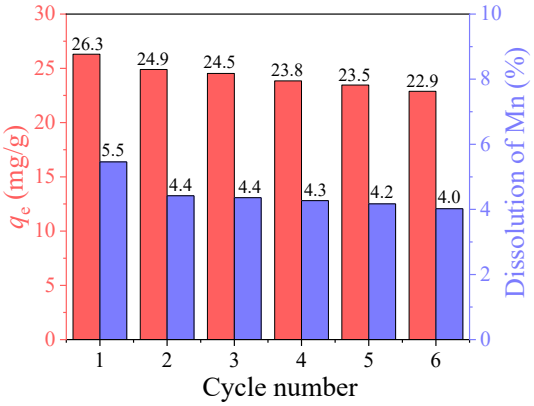

Fig. 11. The Li^+ uptake and loss rate of Mn in each regeneration process.

3.3 Dissolution of Mn

Fig. 12 illustrates the loss rate of Mn and extraction of Li^+ in different content of acid. The dissolution of Mn enhances from 4.4% to 4.6%, and desorption rate of Li^+ improves from 84% to 93% when the content of acid from 0.3 up to 0.6 mol/L. The dissolution of Mn enhances to 5.3% and the desorption of Li^+ reach to 95% in a HCl solution of 1.2 mol/L, indicating the loss rate of Mn and the desorption of Li^+ are improved in stronger HCl environment, which may explained by the Eq. 15 [36].

$$4(Li)[Mn(III)]O_4 + 8H^+ \rightarrow 3(\square)[Mn_2(IV)]O_4 + 4Li^+ + 2Mn(II) + 4H_2O \quad (15)$$

the "□" signifies a vacancy of Li^+.

The extraction rate of Li^+ in r-LMO-Na-2% is 93.7%, which close to the bare r-LMO (94.9%), while the loss rate of Mn is 4.4% and 5.4%, respectively (C_{HCl} = 0.6 mol/L, T = 25°C) are depicted in Fig. S6. The results imply that Mn dissolution can be reduced by trace Na doped, which may due to the obtained Na-O are stronger than Li-O, improving the structure stability. In addition, the amount of Mn^{3+} was decreased by Na doped, which inhibits the Jahn-Teller effect. Both the two parts above can decrease the loss rate of Mn [34].

The influence of temperature on desorption performance as depicted in Fig. S7.

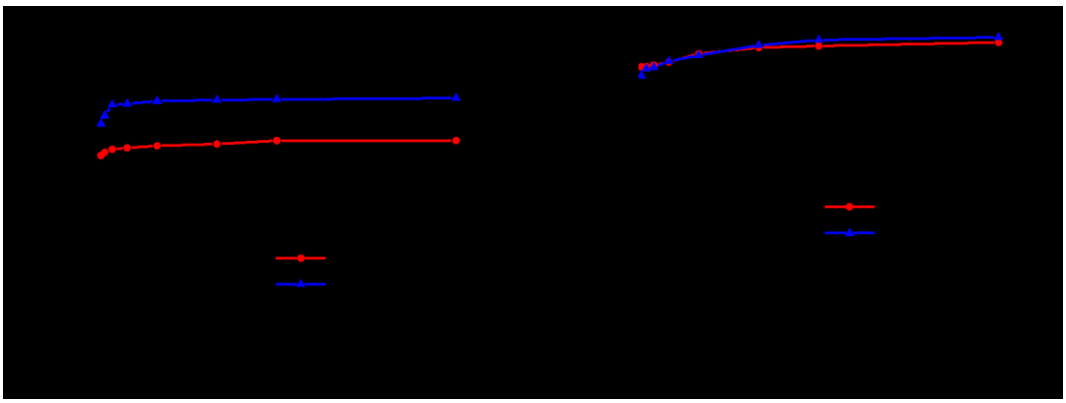

Fig. 12. The desorption processes in different content acid (T = 25°C). (a) Loss rate of Mn and (b) extraction rate of Li^+.

3.4 DFT calculations

3.4.1 The LMO by Na substitute

Theory calculations were carried out to gain more information about the process of surface Na-doping in LMO. The obtained structure of LMO bulk phase and (100) plane were conducted to verify the experimental phenomenon on Na distribution (Fig.

13). A Li at the 16d or 8a site in bulk and at (100) plane was substituted by Na, and related energies were calculated. The results imply that Na atom may substitute Li at the 16d site (-4.15 eV) compare with the 8a site in the bulk (-1.77 eV). Moreover, the △E at the 16d sites of surface (-4.76) is lowest, indicating that the Na may substitute Li on surface 16d sites, consistent with STEM observations [45]. Furthermore, trace Na doping in LMO surface can obtain stronger Na-O bonds, which may improve the structure stability.

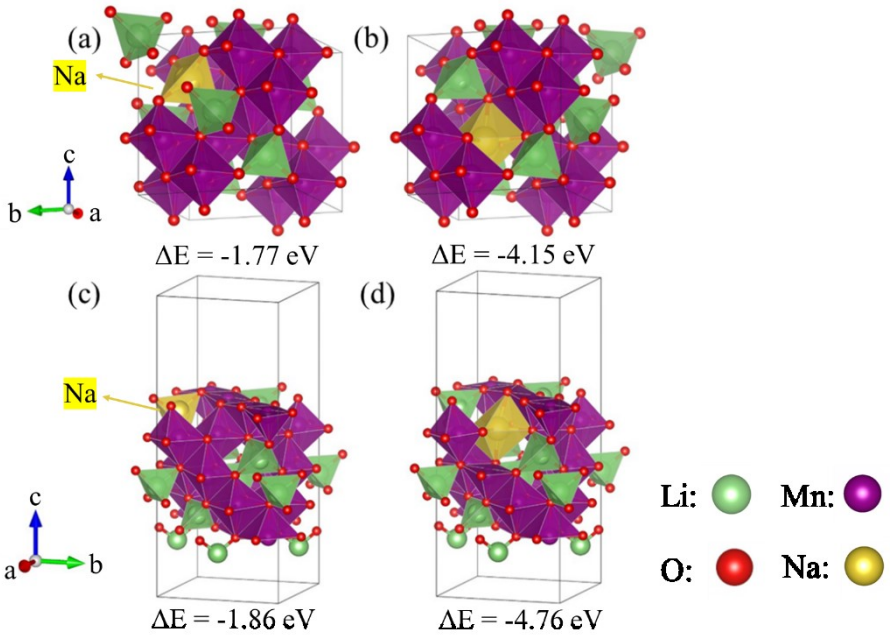

Fig. 13. Optimized structures with doping of Li using Na. (a) 8a, (b) 16d site of Li in bulk. (c) 8a, (d) 16d site of Li on (100) plane.

3.4.2 Density of states

The density of states of bare LMO and the (100) plane by Na doping for Li at the 16d site as depicted in Fig. 14. The results indicate valence band primarily by Mn(d) and O(p) composition, implying there is strong interaction of O and Mn in skeleton structure of [MnO_6] octahedra. Furthermore, the band gap of the (100) surface decrease

to 0.087 eV by Na doped as shown in inset figure from Fig. 14, which is lower obviously than bare LMO (0.17 eV), resulting in improvement electronic conductivity caused by Na doped [46].

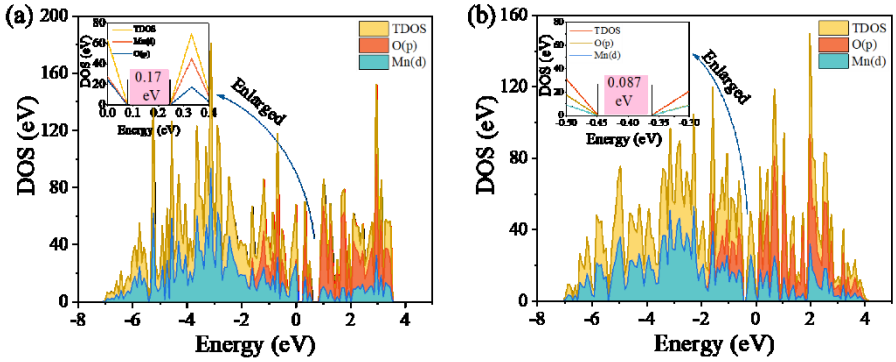

Fig. 14. DOS and PDOS of (a) bare and (b) (100) facet of LMO with Na-doping at a 16d site.

3.4.3 Charge density

The charge density of bare and Na-doped materials as depicted in Fig. 15. The Na doped have little effect on the charge density of 8a sites, while the 16d sites have obvious change. The charge density of the 16d sites is decreased with the Na-doping, which may improve the mean valence state of Mn. So, the anti-dissolution property of Mn is enhanced.

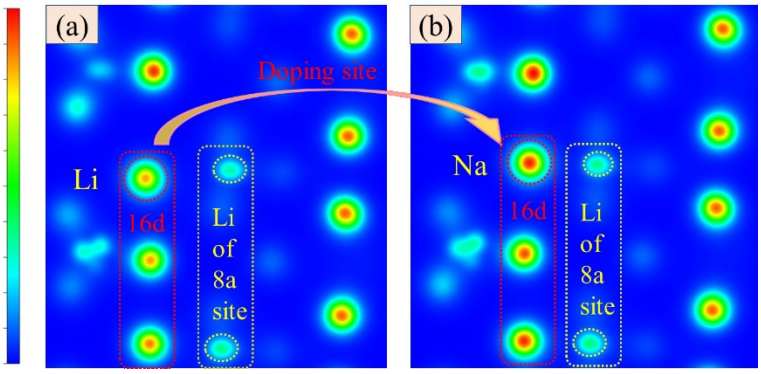

Fig. 15. The charge density of the (a) bare and (b) (100) facet of LMO with Na-doping at the 16d sites.

4 Conclusion

In the present work, we establish a valid method to improve the structure stability and uptake performance of adsorbent by surface Na doping. The Li^+ uptake is enhanced by Na doped (33.9 mg/g) compare to bare HMO (33.5 mg/g), and the Mn dissolution is reduced from 5.4% to 4.4% by Na doped. The materials possess high Li^+ selectivity from Lagoco salt lake and excellent regeneration property. Furthermore, we illustrate the enhancement of the performances of adsorption and anti-dissolution by DFT calculations. The proposed explanations for improving structure stability by surface elements doped will shed lights on further works for Li^+ recovering from solution containing Li^+.

Acknowledgments

A partial support for this work was obtained by the NSFC (No: 51302280 and No: U1607105), the Thousand Talents Plan in Qinghai province, Youth Innovation Promotion Association of Chinese Academy of Sciences (No:2016377), and the Scientific and Technological Funding in Qinghai Province, China (No:2018-GX-101, No:2018-ZJ-722 and No:2019-HZ-808).

References

[1] A.R. Armstrong, P.G. Bruce, Synthesis of layered $LiMnO_2$ as an electrode for rechargeable lithium batteries, Nature, 381 (1996) 499-500.

[2] W.P. Tang, X.J. Yang, Z.H. Liu, K. Ooi, Preparation of β-MnO_2 nanocrystal/acetylene black composites for lithium batteries, J. Mater. Chem. 13 (2003) 2989-2995.

[3] S. Choi, G. Hwang, S. Ilyas, Y. Han, N.V. Myung, B.C. Lee, Y. Song, H. Kim, Inorganic nanofiber as a promising sorbent for lithium recovery, Sep. Purif. Technol. 242 (2020) 116757-116767.

[4] T. Ryu, Y. Haldorai, A. Rengaraj, J. Shin, H.J. Hong, G.W. Lee, Y.K. Han, Y.S. Huh, K.S. Chung, Recovery of lithium ions from seawater using a continuous flow adsorption column packed with granulated chitosan lithium manganese oxide, Ind. Eng. Chem. Res. 55 (2016) 7218-7225.

[5] B. Swain, Recovery and recycling of lithium: A review, Sep. Purif. Technol. 172 (2017) 388-403.

[6] S.Y. Sun, J.L. Xiao, J. Wang, X.F. Song, J.G. Yu, Synthesis and adsorption properties of $Li_{1.6}Mn_{1.6}O_4$ by a combination of redox precipitation and solid-phase reaction, Ind. Eng. Chem. Res. 53 (2014) 15517-15521.

[7] Q.H. Zhang, S.P. Li, S.Y. Sun, X.S. Yin, J.G. Yu, $LiMn_2O_4$ spinel direct synthesis and lithium ion selective adsorption, Chem. Eng. Sci. 65 (2010) 169-173.

[8] F. Yang, S.C. Chen, C.T. Shi, F. Xue, X.X. Zhang, S.G. Ju, W.H. Xing, A facile synthesis of hexagonal spinel lambda-MnO_2 ion-sieves for highly selective Li^+ adsorption, Processes, 6 (2018).

[9] H.J. Hong, I.S. Park, T. Ryu, J. Ryu, B.G. Kim, K.S. Chung, Granulation of $Li_{1.33}Mn_{1.67}O_4$ (LMO) through the use of cross-linked chitosan for the effective recovery of Li^+ from seawater, Chem. Eng. J. 234 (2013) 16-22.

[10] X.J. Yang, H. Kanoh, W.P. Tang, K. Ooi, Synthesis of $Li_{1.33}Mn_{1.67}O_4$ spinels with different morphologies and their ion adsorptivities after delithiation, J. Mater. Chem. 10 (2000) 1903-1909.

[11] W.J. Chung, R.E.C. Torrejos, M.J. Park, E.L. Vivas, L.A. Limjuco, C.P. Lawagon, K.J. Parohinog, S.P. Lee, H.K. Shon, H. Kim, G.M. Nisola, Continuous lithium mining from aqueous resources by an adsorbent filter with a 3D polymeric nanofiber network infused with ion sieves, Chem. Eng. J. 309 (2017) 49-62.

[12] Q. Wang, X. Du, F. Gao, F. Liu, M. Liu, X. Hao, G. Guan, A. Abudula, A novel $H_{1.6}Mn_{1.6}O_4$/reduced graphene oxide composite film for selective electrochemical capturing lithium ions with low concentration, Sep. Purif. Technol. 226 (2019) 59-

67.

[13] L.Y. Tian, W. Ma, M. Han, Adsorption behavior of Li^+ onto nano-lithium ion sieve from hybrid magnesium/lithium manganese oxide, Chem. Eng. J. 156 (2010) 134-140.

[14] F. Ohashi, Y. Tai, Lithium adsorption from natural brine using surface-modified manganese oxide adsorbents, Mater. Lett. 251 (2019) 214-217.

[15] R. Chitrakar, H. Kanoh, Y. Makita, Y. Miyai, K. Ooi, Synthesis of spinel-type lithium antimony manganese oxides and their Li^+ extraction/ion insertion reactions, J. Mater. Chem. 10 (2000) 2325-2329.

[16] Q. Feng, H. Kanoh, Y. Miyai, K. Ooi, Li^+ extraction/insertion reactions with $LiZn_{0.5}Mn_{1.5}O_4$ spinel in the aqueous-phase, Chem. Mater. 7 (1995) 379-384.

[17] R. Chitrakar, Y. Makita, K. Ooi, A. Sonoda, Synthesis of iron-doped manganese oxides with an ion-sieve property: lithium adsorption from bolivian brine, Ind. Eng. Chem. Res. 53 (2014) 3682-3688.

[18] F. Qian, B. Zhao, M. Guo, Z. Qian, N. Xu, Z. Wu, Z. Liu, Enhancing the Li^+ adsorption and anti-dissolution properties of $Li_{1.6}Mn_{1.6}O4$ with Fe, Co doped, Hydrometallurgy, 193 (2020) 105291-105300.

[19] Z. Liu, R.T. Yu, Y.P. Dong, W. Li, B.L. Lv, The adsorption behavior and mechanism of Cr(VI) on 3D hierarchical α-Fe_2O_3 structures exposed by (001) and non-(001) planes, Chem. Eng. J. 309 (2017) 815-823.

[20] L.F. Chen, X. Xu, J.J. Song, X.D. Zhu, Z.W. Qi, Microwave assisted hydrothermal synthesis of MnO_2 center dot $0.5H_2O$ ion-sieve for lithium ion selective adsorption, Sep. Sci. Technol. 51 (2016) 874-882.

[21] J.L. Xiao, X.Y. Nie, S.Y. Sun, X.F. Song, P. Li, J.G. Yu, Lithium ion adsorption-desorption properties on spinel $Li_4Mn_5O_{12}$ and pH-dependent ion-exchange model, Adv. Powder Technol. 26 (2015) 589-594.

[22] Z.Q. Jiang, X. Gu, L.X. Wang, L. Huang, First-principles study of intercalation of alkali ions in FeSe for solid-state batteries, Chem. Phys. Lett. 659 (2016) 230-233.

[23] P.Y. Ji, C.S. Zhang, J. Wan, M.L. Zhou, Y. Xi, H.Y. Guo, C.G. Hu, X. Gu, C.S. Wang, W.D. Xue, Ti-doped tunnel-type $Na_4Mn_9O_{18}$ nanoparticles as novel anode

materials for high-performance supercapacitors, ACS Appl. Mater. Inter. 11 (2019) 28900-28908.

[24] J.N. Reimers, E.W. Fuller, E. Rossen, J.R. Dahn, Synthesis and electrochemical studies of $LiMnO_2$ prepared of low-temperatures, J. Electrochem. Soc. 140 (1993) 3396-3401.

[25] A.L. Gao, Z.H. Sun, S.P. Li, X.J. Hou, H.Q. Li, Q.S. Wu, X.G. Xi, The mechanism of manganese dissolution on $Li_{1.6}Mn_{1.6}O_4$ ion sieves with HCl, Dalton Tran, 47 (2018) 3864-3871.

[26] S. Liu, Z.P. Liu, X. Shen, W.H. Li, Y.R. Gao, M.N. Banis, M.S. Li, K. Chen, L. Zhu, R.C. Yu, Z.X. Wang, X.L. Sun, G. Lu, Q.Y. Kong, X.D. Bai, L.Q. Chen, Surface doping to enhance structural integrity and performance of Li-rich layered oxide, Adv. Energy Mater. 8 (2018).

[27] R. Chitrakar, H. Kanoh, Y. Miyai, K. Ooi, A new type of manganese oxide (MnO_2 center dot $0.5H_2O$) derived from $Li_{1.6}Mn_{1.6}O_4$ and its lithium ion-sieve properties, Chem. Mater. 12 (2000) 3151-3157.

[28] Y.M. Hon, H.Y. Chung, K.Z. Fung, M.H. Hon, NMR and FT-IR investigation of spinel $LiMn_2O_4$ cathode prepared by the tartaric acid gel process, J. Solid State Chem. 160 (2001) 368-376.

[29] Z.Y. Ji, M.Y. Zhao, Y.Y. Zhao, J. Liu, J.L. Peng, J.S. Yuan, Lithium extraction process on spinel-type $LiMn_2O_4$ and characterization based on the hydrolysis of sodium persulfate, Solid State Ionics, 301 (2017) 116-124.

[30] S.H. Ye, J.K. Bo, C.Z. Li, J.S. Cao, Q.L. Sun, Y.L. Wang, Improvement of the high-rate discharge capability of phosphate-doped spinel $LiMn_2O_4$ by a hydrothermal method, Electrochim. Acta, 55 (2010) 2972-2977.

[31] M. Helan, L.J. Berchmans, T.P. Jose, A. Visuvasam, S. Angappan, Molten salt synthesis of $LiMn_2O_4$ using chloride-carbonate melt, Mater. Chem. Phys. 124 (2010) 439-442.

[32] C.Y. Tang, K. Leung, R.T. Haasch, S.J. Dillon, $LiMn_2O_4$ surface chemistry evolution during cycling revealed by in situ auger electron spectroscopy and X-ray photoelectron spectroscopy, ACS Appl. Mater. Inter. 9 (2017) 33968-33978.

[33] X.B. Luo, K. Zhang, J.M. Luo, S.L. Luo, J. Crittenden, Capturing lithium from wastewater using a fixed bed packed with 3-D MnO_2 Ion Cages, Environ. Sci. Technol. 50 (2016) 13002-13012.

[34] G.F. Cao, X.Y. Yang, Z.L. Yin, Y.T. Lei, H. Wang, J.S. Li, Synthesis, adsorption properties and stability of Cr-doped lithium ion sieve in salt lake brine, B. Chem. Soc. Jpn. 92 (2019) 1205-1210.

[35] K. Ooi, Y. Miyai, J. Sakakihara, Mechanism of Li^+ insertion in spinel-type manganese oxide. Redox and ion-exchange reactions, Langmuir, 7 (1991) 1167-1171.

[36] X. Xu, Y. Chen, P. Wan, K. Gasem, K. Wang, T. He, H. Adidharma, M. Fan, Extraction of lithium with functionalized lithium ion-sieves, Prog. Mater. Sci. 84 (2016) 276-313.

[37] X.C. Shi, D.F. Zhou, Z.B. Zhang, L.L. Yu, H. Xu, B.Z. Chen, X.Y. Yang, Synthesis and properties of $Li_{1.6}Mn_{1.6}O_4$ and its adsorption application, Hydrometallurgy, 110 (2011) 99-106.

[38] D.L. Gu, W.J. Sun, G.F. Han, Q. Cui, H.Y. Wang, Lithium ion sieve synthesized via an improved solid state method and adsorption performance for West Taijinar Salt Lake brine, Chem. Eng. J. 350 (2018) 474-483.

[39] Z. Liu, Y.Q. Zhou, M. Guo, B.L. Lv, Z.J. Wu, W.Z. Zhou, Experimental and theoretical investigations of Cs^+ adsorption on crown ethers modified magnetic adsorbent, J. Hazard. Mater. 371 (2019) 712-720.

[40] N.S. Surgutskaia, A.D. Martino, J. Zednik, K. Ozaltin, L. Lovecká, E.D. Bergerová, D. Kimmer, J. Svoboda, V. Sedlarik, Efficient Cu^{2+}, Pb^{2+} and Ni^{2+} ion removal from wastewater using electrospun DTPA-modified chitosan/polyethylene oxide nanofibers, Sep. Purif. Technol. 247 (2020).

[41] M. Aliabadi, M. Irani, J. Ismaeili, H. Piri, M.J. Parnian, Electrospun nanofiber membrane of PEO/Chitosan for the adsorption of nickel, cadmium, lead and copper ions from aqueous solution, Chem. Eng. J. 220 (2013) 237-243.

[42] G.M. Nisola, L.A. Limjuco, E.L. Vivas, C.P. Lawagon, M.J. Park, H.K. Shon, N. Mittal, I.W. Nah, H. Kim, W.J. Chung, Macroporous flexible polyvinyl alcohol

lithium adsorbent foam composite prepared via surfactant blending and cryo-desiccation, Chem. Eng. J. 280 (2015) 536-548.

[43] F.R. Qian, M. Guo, Z.Q. Qian, Q. Li, Z.J. Wu, Z. Liu, Highly lithium adsorption capacities of $H_{1.6}Mn_{1.6}O_4$ ion-sieve by ordered array structure, Chemistryselect, 4 (2019) 10157-10163.

[44] Q. Feng, H. Kanoh, Y. Miyai, K. Ooi, Hydrothermal synthesis of lithium and sodium manganese oxides and their metal-ion extraction insertion reactions, Chem Mater, 7 (1995) 1226-1232.

[45] J.N. Zhang, Q.H. Li, C.Y. Ouyang, X.Q. Yu, M.Y. Ge, X.J. Huang, E.Y. Hu, C. Ma, S.F. Li, R.J. Xiao, W.L. Yang, Y. Chu, Y.J. Liu, H.G. Yu, X.Q. Yang, X.J. Huang, L.Q. Chen, H. Li, Trace doping of multiple elements enables stable battery cycling of $LiCoO_2$ at 4.6V, Nat. Energy, 4 (2019) 594-603.

[46] Q. Gan, H. He, Y. Zhu, Z. Wang, N. Qin, S. Gu, Z. Li, W. Luo, Z. Lu, Defect-assisted selective surface phosphorus doping to enhance rate capability of titanium dioxide for sodium ion batteries, ACS Nano, 13 (2019) 9247-9258.